Self-assembled artificial pinning centres in thick YBCO superconducting films

2010 J. Phys.: Conf. Ser. 234 022022

(http://iopscience.iop.org/1742-6596/234/2/022022)

Journal of Physics: Conference Series **234** (2010) 022022 doi:10.1088/1742-6596/234/2/022022

Self-assembled artificial pinning centres in thick YBCO superconducting films

P. Mikheenko[1], **J. S. Abell**[1], **A. Sarkar**[1], **V.S. Dang**[1], **M.M. Awang Kechik**[1], **J.L. Tanner**[1], **P. Paturi**[2], **H. Huhtinen**[2], **N. Hari Babu**[3], **D. A. Cardwell**[3], and **A. Crisan**[1,4]

[1] School of Metallurgy and Materials, University of Birmingham, Birmingham B15 2TT , UK

[2] Wihuri Physical Laboratory, Department of Physics and Astronomy, FI-20014 University of Turku, Finland

[3] Department of Engineering, Cambridge University, Cambridge CB2 1PZ, UK

[4] National Institute of Materials Physics, Bucharest 077125, Romania

[a] E-mail: p.mikheenko@bham.ac.uk

Abstract. Strong, artificial pinning centres are required in superconducting films of large thickness for power applications in high magnetic fields. One of the methods for the introduction of pinning centres in such films is substrate decoration, i.e., growing nanoscale islands of certain materials on the substrate prior to the deposition of the superconducting film. Two other methods are building up a layered distribution of a second phase and homogeneous incorporation of second phase inclusions from a compositional target. In this paper, we compare the effectiveness of these methods in terms of the type of the self-assembly of nanoparticles. The comparison is made over a large set of $YBa_2Cu_3O_7$ films of thickness up to 6.6 μm deposited with Au, Ag, Pd, $LaNiO_3$, $PrBa_2Cu_3O_7$, YBCO, $BaZrO_3$ and $Gd_2Ba_4CuWO_y$ nanoparticles. It is found that substrate-decoration self-assembly is able to provide higher critical current in low magnetic field than the incorporation of homogeneous second phase in the sample microstructure. By specific modification of substrate decoration we achieved the self-field critical current per centimetre of width of 896 A/cm at 77.3 K and 1620 A/cm at 65 K in a film of thickness of 4.8 μm.

Introduction

High-current superconducting applications depend strongly on the performance of superconducting tapes. Superconducting tapes, for example, are expected to find a wide use in power transmission lines, magnets, motors, generators, transformers, fault current limiters etc. In these applications they can be exposed to a high magnetic field. To increase the in-field performance of the tapes, it is necessary to incorporate into their microstructure a very dense, nanometer scale, array of pinning centers. A range of different methods for creating such an array using nanoparticles has been suggested and explored. Among these methods are substrate decoration [1], a quasi-superlattice approach [2] and volumetric addition of a secondary phase [3]. Self-assembly of nanoparticles plays an important role in each of these techniques. The first two methods represent two-dimensional (2D) and the third a three-dimensional (3D) approach to self-assembly.

[a] To whom any correspondence should be addressed.

In this work, we compare the effectiveness of 2D and 3D self-assembly in increasing critical current per centimeter of width ($I_{c\text{-}w}$) in $YBa_2Cu_3O_7$ (YBCO) thick films. The 2D self-assembly has been achieved in films containing Ag, Au, Pd, YBCO, $PrBa_2Cu_3O_x$ and $LaNiO_3$ nanoparticles. The 3D self-assembly was assessed using $Gd_2Ba_4CuWO_x$ and $BaZrO_3$ nanoparticles. All the nanoparticles investigated showed significant potential to increase $I_{c\text{-}w}$ [4-8] to levels above that observed in pure YBCO films.

The increase of the thickness (d) in pure YBCO films results in a decrease of critical current density $J_c=I_c/dw$, where I_c is critical current and w is the width of the film. An important contribution to this process is the high-temperature annealing of defects that are able to pin magnetic flux [9]. The nanoparticles, if introduced in the film, can play a dual role. They can pin magnetic flux directly and can also generate associated defects in the film that form effective flux pinning sites. A degree of order in the distribution of nanoparticles could make pinning of defects more effective than a stochastic distribution. We argue that the type of self-assembly that introduces such order plays an important role in the increase of $I_{c\text{-}w}$ given that it defines the final position of nanoparticles in the film.

We found that films of several micrometers thickness with artificially introduced nanoparticles can compete successfully with pure YBCO films. The self-organized features in the distribution of nanoparticles provide specific nano-scale defect structure, which results in an enhancement of $I_{c\text{-}w}$ in a particular magnetic field. The value of this field is typically in the range of few tesla and can be tuned by changing the size and density of the defects according to the needs of a specific high current application. In this respect, nanoparticles provide an element of control that is absent in pure YBCO films. The main conclusion of this study is that the specific type of self-assembly of nanoparticles plays a key role in determining the resulting superconducting properties of the tapes in magnetic field along the c-axis of YBCO. In addition, for selected set of samples, a 2D self-assembly can be more effective in supporting high $I_{c\text{-}w}$ in low field than a 3D self-assembly.

Experimental

Pulsed laser deposition (PLD) was used for the growth of YBCO and the deposition of nanoparticles. Ag, Au, Pd, $PrBa_2Cu_3O_x$ and $LaNiO_3$ nanoparticles were deposited from respective targets in a two-target configuration (one being commercial YBCO), while $Gd_2Ba_4CuWO_x$ and $BaZrO_3$ were incorporated in the target and deposited simultaneously with YBCO. The deposition of YBCO was carried out in a chamber with base pressure of 10^{-6} Torr. An excimer KrF 248 nm laser with pulse duration of 30 ns, repetition rate of 4-8 Hz and laser energy density of 0.67 J/cm^2 was used to ablate the target material. The target-substrate distance was 5.6 cm. The substrate temperature for YBCO growth was set to 780 °C and the oxygen partial pressure during the deposition was 450 mTorr. Several different substrate temperatures in the range 200-780 °C were used for the deposition of nanoparticles. After final deposition of YBCO, films were cooled down at the rate of 10 °C/min in partial oxygen pressure of 450 Torr. The films of the thickness up to 6.6 µm have been prepared.

In the substrate-decoration method, one layer of nanoparticles was deposited on the substrate prior the growth of YBCO. In the quasi-superlattice approach, several (up to 20) layers of nanoparticles were deposited between the YBCO layers of different thickness.

We investigated the surface topography of the nano-dots on the substrate by atomic force microscopy (AFM) using high resolution AFM probes with diameter of curvature of 1-10 nm. The AFM pictures were analysed by WSxM 4.0 software. AFM imaging was also used to investigate the top surface or a cleaved cross section of the films.

The films were fully characterised using a Quantum Design 5-Tesla Magnetic Property Measurement System MPMS-XL and a 7 T Physical Property Measurement System. A large number of samples were investigated as part of this study. Critical temperatures of the films, defined as the temperature of the peak of imaginary alternating current (AC) susceptibility at low amplitude of AC field of 0.5 Oe, were measured and observed to vary typically from 89 to 91 K. The critical current for the magnetic field (H) along the c-axis of the film was derived from the direct-current (DC) magnetic moment [4] and was analysed as a function of magnetic field at a fixed temperature in the range of 5 - 77.3 K. The I_c for directions of applied magnetic field other than along the c-axis was determined by

angle-dependent transport measurements on microbridges patterned using conventional photolithography.

Scanning and transmission electron microscopy (SEM, TEM) and energy dispersive x-ray analysis (EDX) were used to analyse element content, micro- and nanostructure of the samples.

Results and discussion

Substrate decoration is an example of 2D self-assembly of nanoparticles. Two examples of Au nanoparticles on a $SrTiO_3$ (STO) substrate are shown in Figs. 1 and 2. In Fig. 1, Au nanoparticles were deposited with 25 laser pulses at a temperature of 780 °C. The nanoparticles, which were self-assembled from the Au plasma, form truncated oblate spheroids and cover most of the area of the substrate. To achieve self-organizing features, the number of laser pulses was increased to obtain a complete single-layer coating of the substrate with dense packaging of nanoparticles (see Fig. 2).

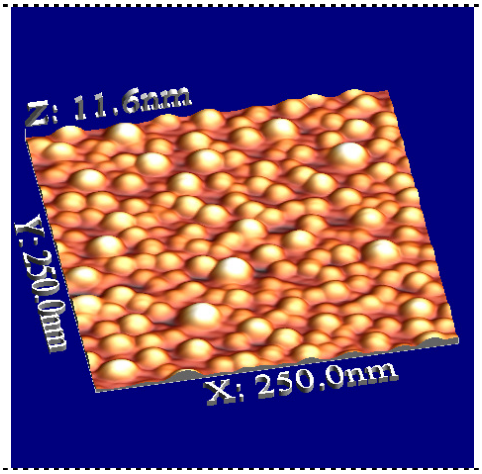

Figure 1. Three-dimensional AFM image of Au nanoparticles on a STO substrate deposited with 25 laser pulses at 780 °C. The height of the pixels scales with planar sizes in the image.

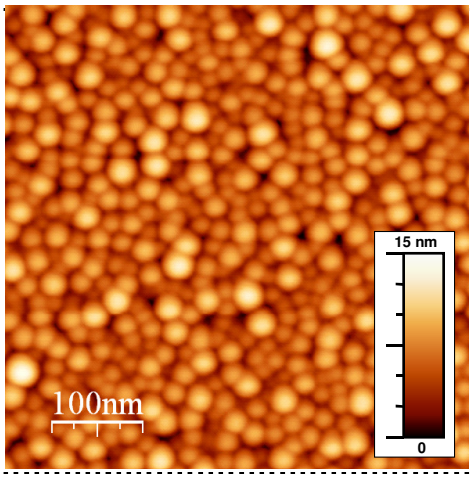

Figure 2. Two-dimensional AFM image of Au nanoparticles on STO substrate deposited with 50 laser pulses at 780 °C. A dense, single-layer coating is achieved. The inset shows the height of pixels in nanometres.

Nanoparticles of other materials were observed to form a similar architecture, but typically require lower substrate temperatures. As a result, temperatures of 200–400 °C were used to deposit Ag, Pd, YBCO, $PrBa_2Cu_3O_x$ and $LaNiO_3$ nanoparticles. The size of the nanoparticles is different for different materials and temperatures of deposition. For example, Ag nanoparticles deposited at 200 °C are about half the size of the Au nanoparticles shown in Fig. 2 and single-layer coating is achieved after only fifteen laser pulses. At least for Au and Ag nanodots, a dense, single-layer coating produces the highest $I_{c\text{-}w}$ compared to other coatings.

This study raises an important question regarding the growth mechanism of epitaxial, high-I_c YBCO films on a coated substrate, such as that shown in Fig. 2. The surface of this substrate is not smooth and the lattice parameters of the coating material are different to those of YBCO. Even so, x-ray and electron backscatter diffraction confirm that the resulting YBCO films are single-crystalline and epitaxial to the underlying STO substrate. The answer may relate to the specific growth mechanism described in the literature [10] for the growth of single crystalline whiskers [11]. In this process, material grows epitaxially on a flat bottom surface moving constantly upwards. Particles of a different size would move at a different speed and may be overgrown with YBCO, as observed in the TEM image shown in Fig. 3. Several Ag nanoparticles in this figure are marked by arrows. These extend from the YBCO/STO interface to an average distance of about 200 nm. The particles create vertical defects originating from their edges when they are overgrown by YBCO. These defects, such as that above the Ag nanoparticle marked as 1 in Fig.3, are clearly visible.

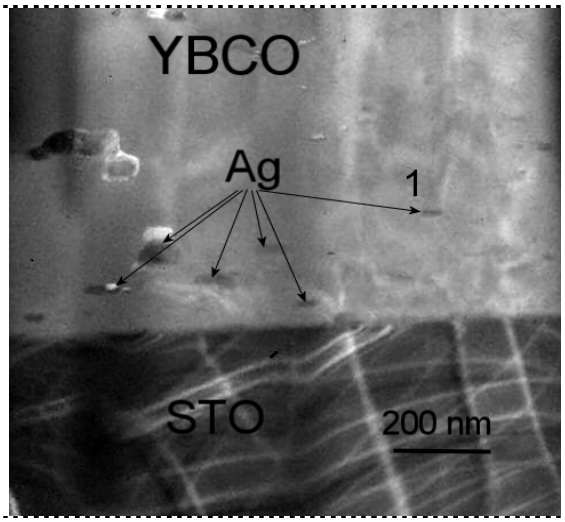

Figure 3. TEM image of YBCO/STO interface of an YBCO film on STO substrate decorated with Ag nanoparticles (marked by arrows). The nanoparticles move towards the surface of the film.

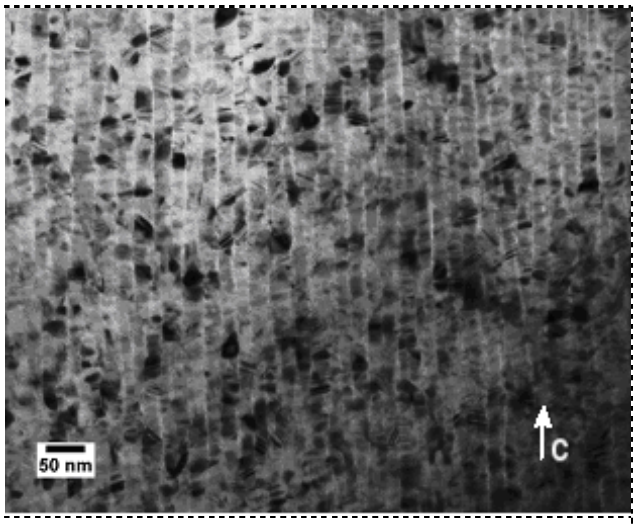

Figure 4. TEM image of a cross-sectional area inside an YBCO/Ag film similar to that shown in Fig.3. A regular nanometre-scale columnar structure is evident in the image. The direction of c-axis of YBCO is shown in the bottom right corner of the image.

Defects originating in this way are effectively pinned by the nanoparticle from which they originate and are retained within the film. Under appropriate conditions, the structure of YBCO above the nanoparticles demonstrates a nearly perfect columnar structure, as shown in Fig. 4. The variation in contrast in this figure is due to different local thickness of TEM sample. The structure in Fig. 4 resembles the columnar structure observed in MgB_2 films [12]. Similar columnar features are seen in the cross-sectional AFM image in Fig. 5. The films with columnar structure show secondary, *c*-axis, peaks in the angle-dependent transport measurements (Fig. 6). Although there is no evidence that this columnar structure is present everywhere in the film, the films containing such columnar defects show superior $I_{c\text{-}w}$, which is above that for pure YBCO reference films deposited as part of this study.

The angular dependence of critical current density for another system, Au-decorated YBCO, is shown in Fig. 7. The measurements were performed at temperature of 77.3 K and different magnetic fields of 3-6 T (shown in the plot). The Au nanoparticles are less successful for decoration than Ag nanoparticles. Although some improvement of J_c in the field along the *c*-axis is obvious, it is not as strong as for Ag nanoparticles. In contrast to Fig. 6, the decrease in J_c in field along the *c*-axis observed in Fig. 7 is by more than two orders of magnitude. The behaviour in the field along the *ab*-plane in Figs. 6 and 7 is similar. This suggests that improvement in J_c is mainly along the *c*-axis, as reported in the paper by Maiorov et al. [13].

In addition to Au and Ag, 2D self-assembly of Pd, non-superconducting YBCO (nsYBCO) [8], $PrBa_2Cu_3O_x$ and $LaNiO_3$ was also used to generate defects in YBCO films. The nanoparticles of these materials were grown at temperatures of 200-400 °C. The growth of YBCO film in the presence of nsYBCO, $PrBa_2Cu_3O_x$ and $LaNiO_3$ nanoparticles is most likely to be described by a more complicated scenario than with nanoparticles of pure metals.

We believe that the advantage of 2D self-assembly is the low quantity of material required for the growth of the film (compared, for example, with building gold nanorods in the films described in ref. [14]). In 2D self-assembly, the main feature of the nanoparticles is not to pin vortices but to create and pin extended defects in the sample. A quasi-superlattice approach was used to introduce more defects, which involved periodically adding more nanoparticles after growing layers of YBCO. The images in Figs. 3 and 4 were taken from the resulting Ag/YBCO quasi-superlattices.

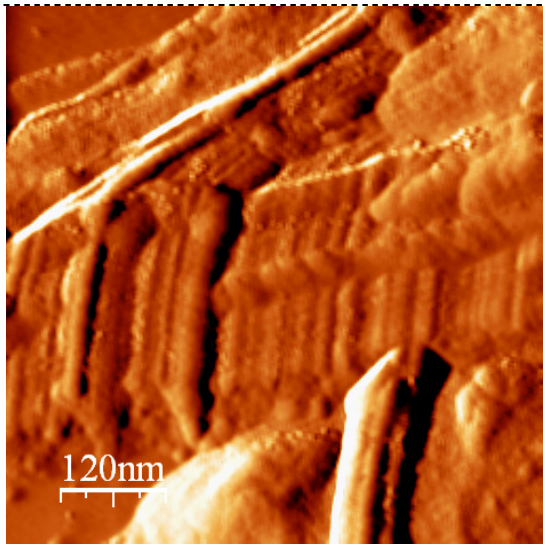

Figure 5. Cross-sectional AFM image of an YBCO film on STO substrate decorated with Ag nanoparticles. Vertical YBCO columns of diameter of about 20 nm are evident in the image.

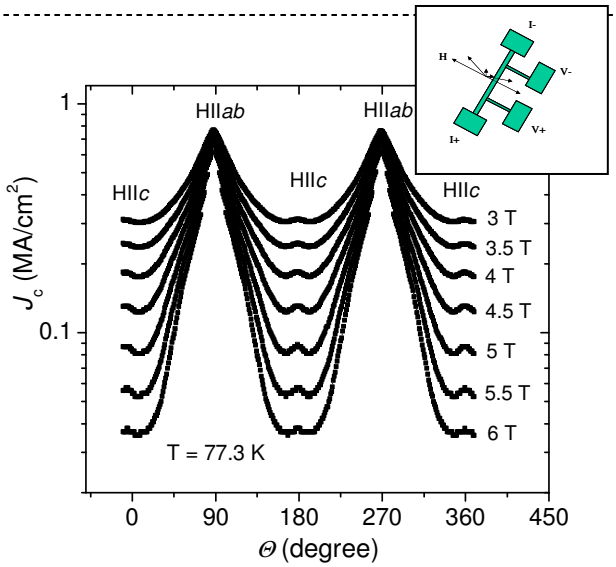

Figure 6. Angular dependence of critical current density at 77.3 K and different magnetic fields (shown in the plot) for a sample similar to that in Fig. 5. The peaks at 0, 180 and 360° are due to the columnar structure of YBCO. The sample configuration is shown in the inset.

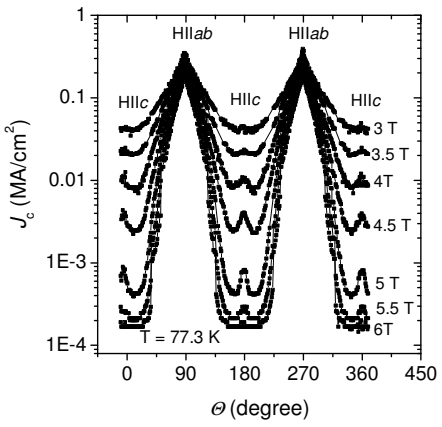

Figure 7. Angular dependence of critical current density for an Au-decorated YBCO sample. The measurements were performed at temperature of 77.3 K and different magnetic fields of 3-6 T. The peaks at 0, 180 and 360° are due to the columnar structure of YBCO.

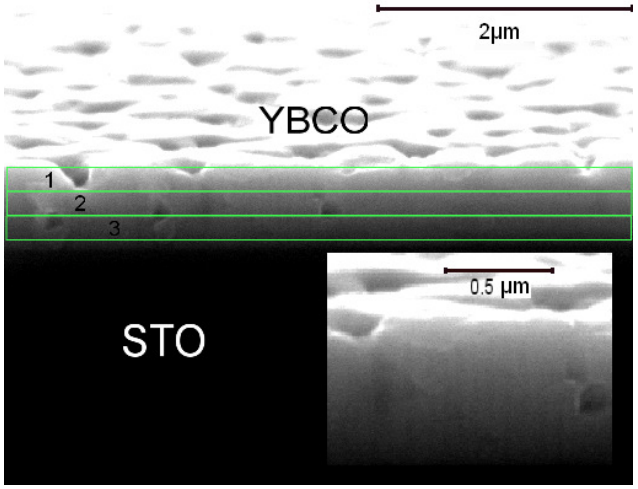

Figure 8. Cross-section of a YBCO film containing Gd2411 nanoparticles. The green boxes 1-3 are the areas chosen for the EDX analyses. The inset shows a magnified area of the cross-section. The dark vertical lines may represent contrast from the extended defects created by Gd2411 nanoparticles.

Another approach to enhance $I_{c\text{-}w}$ is 3D self-assembly. This was investigated using $Gd_2Ba_4CuWO_x$ (Gd2411) and $BaZrO_3$ (BZO) nanoparticles. In this approach, the nanoparticles assemble in the film in the presence of YBCO. Evidence for the motion of Gd2411 from cross-sectional SEM was observed in a similar way to the motion of nanoparticles in 2D self-assembly. In this case, however, nanoparticles move towards the substrate.

Fig. 8 shows a cross-section of YBCO film deposited from an YBCO target with added 1 mol. % of Gd2411. The area of the cross-section was divided into three rectangular sections marked 1-3 and the element analysis was performed in these sections in order to clarify distribution of Gd2411 along the direction normal to the plane of the film. As a control measure, element analysis was taken from the surface of the film, concentrating on the atomic percentage of Gd.

Analysis of the surface of the film gives an atomic Gd content of 1.08 %. The percentage of Gd in the sections 1, 2 and 3 is 1.39, 2.01 and 3.66 %, respectively. This indicates that the motion of Gd2411 nanoparticles is towards the substrate. The nanoparticles may join each other during this process to form extended defects and improve pinning along the c-axis of YBCO.

The angular dependence of critical current density at 77.3 K and magnetic field of 5 T for a sample containing Gd2411 nanoparticles is shown in Fig. 9. We believe that a small peak at 180° is related to columnar defects seen in the inset of Fig. 8.

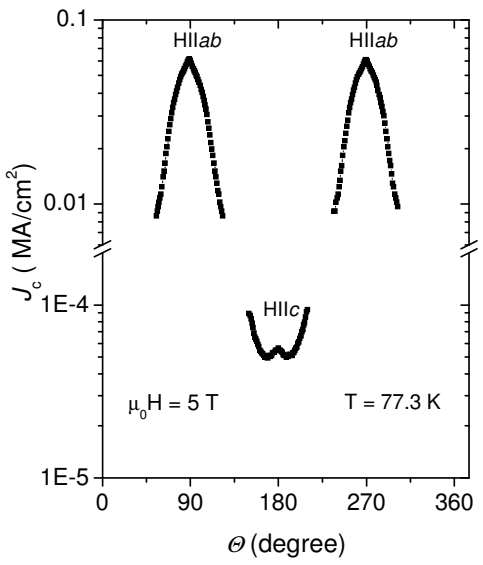

Figure 9. Angular dependence of critical current density at 77.3 K and magnetic field of 5 T for a sample containing Gd2411 nanoparticles. A small peak at 180° might be due to columnar defects seen in Fig. 8.

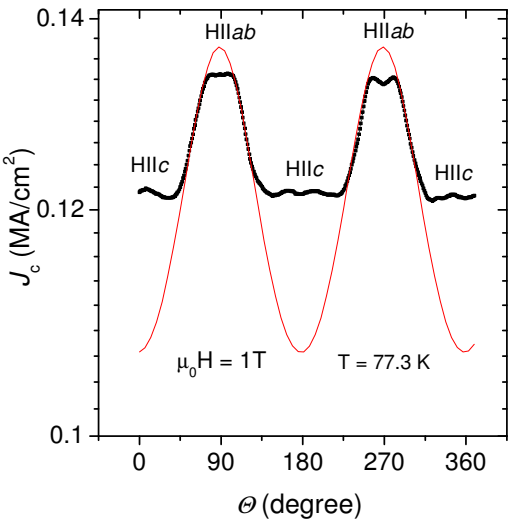

Figure 10. Angular dependence of critical current density at 77.3 K and magnetic field of 1 T for a sample containing BZO nanoparticles. The sample demonstrates very low anisotropy. The thin red line shows a fitting curve for the pinning on point defects.

A large number of nano-structured films of another 3D self-assembling system based on BZO have been grown and studied in this work. A bamboo-like defect structure, effective for pinning of vortices, appears at high temperature or slow rate of deposition [15]. The properties of our BZO+YBCO films are in agreement with the results reported elsewhere [15-21]. Fig. 10 shows an angular dependence of critical current density at 77.3 K and magnetic field of 1 T for a sample containing BZO nanoparticles. The sample exhibits very low anisotropy. The thin red line shows a

fitting curve for the pinning on point defects, which takes into account mass anisotropy of charge carriers in YBCO. The difference between experimental data and the curve fit reflects effect of extended defects that contribute to the pinning along *c*-axis of the film. The complicated form of the curve is due to the specific splayed arrangement of sections of BZO columns [15].

A summary of our results for representative samples with different nanoparticles is shown in the Table 1. The table includes information about layered structure, film thickness, critical current per centimetre of width at zero magnetic field ($I_{c\text{-}w}(0)$) and field of 1 T ($I_{c\text{-}w}(1T)$), and the maximum volume pinning force F_p^{max} at temperature of 77.3 K. It is also worth mentioning $I_{c\text{-}w}(0)$ and $I_{c\text{-}w}(1T)$ for YB4 at 65 K, which are 1620 and 294 A/cm, respectively, and $I_{c\text{-}w}(0)$ for DA20 and DA19 at 70 K that are 1156 and 1144 A/cm, respectively. The values of $I_{c\text{-}w}(0)$ for these samples are above those of state-of-the-art films with nanoparticles reported in literature [3, 15-25] and also pure YBCO films. For example, $I_{c\text{-}w}(0)$ of about 390 A/cm at 77 K is reported in [17] and ~670 A/cm in [20]. We believe that this is due to a very small amount of external phase of nanoparticles sufficient for formations of defects in YBCO. A larger amount would negatively affect crystallinity and chemical composition of the films.

Table 1. Parameters of YBCO films at temperature 77.3 K. *d* is thickness of the film, $I_{c\text{-}w}(0)$ is critical current per centimetre of width at zero magnetic field, $I_{c\text{-}w}(1T)$ is critical current per centimetre of width at magnetic field of 1 T, F_p^{max} is maximum volume pinning force. The layer structure shows the sequence and number of laser pulses.

Sample	Layer structure	*d* (μm)	$I_{c\text{-}w}(0)$ (A/cm)	$I_{c\text{-}w}(1T)$ (A/cm)	F_p^{max} (GN/m^3)
YB4	($YBCO_n$20/YBCO5000)x3	4.8	896	84	3.6
DA20	(Ag25;35;45/ YBCO5000)x3	4.8	820	65	2.6
DA19	(Ag25;35/ YBCO5000)x2	3.2	659	59	3.6
PY9	(Pd15/ YBCO5000)x2	3.33	530	46	1.4
NO10	LNO10/ YBCO5000	1.65	358	31	1.9
DP2	(PBCO20/ YBCO5000)x2	1.3	289	16	1.6
FT153	Au50/ YBCO5000	0.8	255	14	1.8
M70	(BZO+YBCO)5000	1.28	237	47	6.1
DB92	(BZO+YBCO)10000	2.4	234	67	3.1
M33	(Gd2411+YBCO)5000	0.8	216	10	1.4

Other results are presented in Fig. 8 (in logarithmic scale) in the form of $I_{c\text{-}w}$ as the function of magnetic field along the *c*-axis for the best and typical YBCO films, films with 2D self-assembly (Ag and nsYBCO nanoparticles) and 3D self-assembly (BZO and Gd2411). The measurements were made at a temperature of 77.3 K. The low-field I_c of best samples is close to 1 kA/cm, which is a benchmark and target for superconducting tapes. For other temperatures, one of the samples exceeds 1 kA/cm at 75.5 K, frequently used in measurements of J_c and $I_{c\text{-}w}$ [3,15,21,25], and three films exceed this value at 70 K.

The Gd2411 nanoparticles containing a mainly diffuse 3D arrangement exhibit the lowest I_c. The BZO nanoparticles demonstrate high critical current density over the entire measured field range. In terms of total current per centimetre of width, however, this matches $I_{c\text{-}w}(H)$ of the best pure YBCO films prepared as part of this study. The highest $I_{c\text{-}w}$ exceeding that of any pure YBCO film is observed here in the samples with 2D self-assembly only. For better clarity, the inset to Fig. 11 shows $I_{c\text{-}w}(H)$ in linear scale in a range of low and moderate magnetic fields.

It can be seen from Table 1 and Fig. 8, that in spite of high $I_{c\text{-}w}(0)$, $I_{c\text{-}w}(1T)$ in the 2D self-assembly samples is below the values of most state-of-the-art films, especially with BZO nanoparticles [3, 15-

25]. In the samples with 2D self-assembly, the ratio $I_{c\text{-}w}(0)/I_{c\text{-}w}(1T)$ is above 10, while in the samples with BZO it is typically 3 to 5. The advantage in high field of the films containing BZO or similar nanoparticles is that they are able to form both columnar and point-like defects [15]. Although there is a sufficient number of defects in clean columnar films like that shown in Fig. 4, they cannot effectively counteract thermal fluctuations and exhibit relatively low F_p^{max}. Even so, we believe that films of such a regular structure can be grown to a thickness higher than films with BZO, without displaying a degraded top layer, such as that reported in ref. [21]. Also, there is difference in the frequency dependence of critical current for these two groups of samples. We measured $I_{c\text{-}w}$ of the samples in high field in the range of frequencies from 47 to 10000 Hz. We found that the increase in $I_{c\text{-}w}$ with frequency is stronger in 2D-based samples than in BZO self-assembled ones. For example, at 4 T, the ratio of $I_{c\text{-}w}$ at 10000 and 47 Hz is 17 for a 2D Ag-based sample and 7 for an optimised BZO+YBCO sample. Based on these findings, we believe that YBCO tapes grown on 2D self-assembled nanoparticles will find use in power applications that do not involve high magnetic fields or use high frequency superconducting currents.

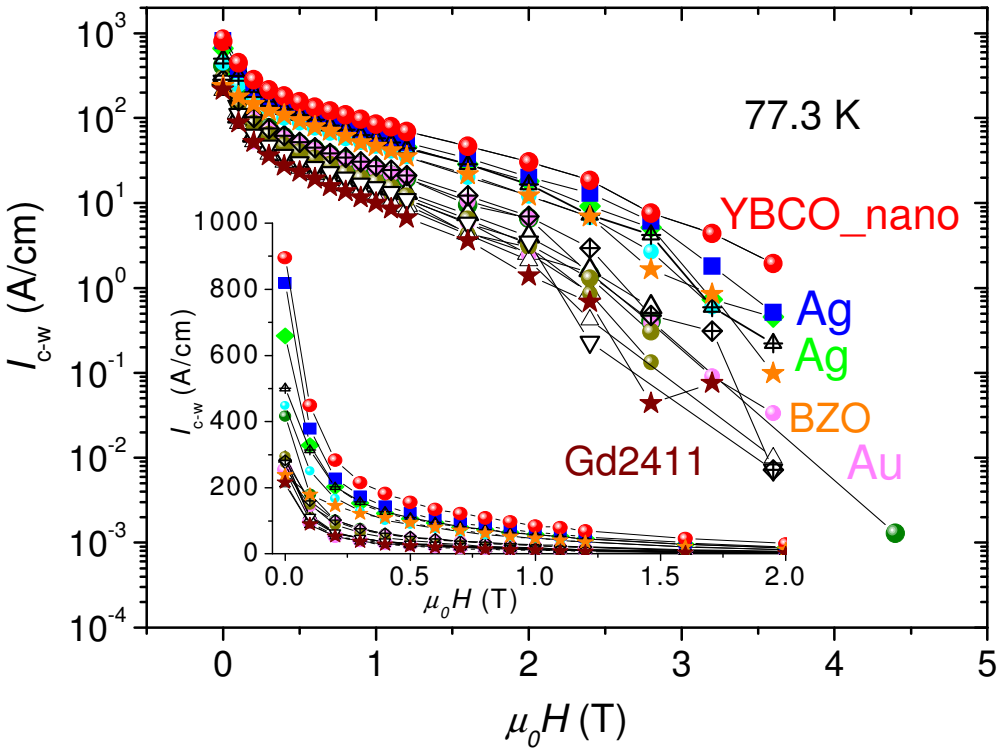

Figure 11. Field dependence of critical current per centimetre of width for a range of typical and best YBCO films with 2D and 3D self-assembled nanoparticles. The black open symbols show $I_{c\text{-}w}(B)$ for pure YBCO films. The brown and orange stars are for the 3D self-assembled Gd2411 and BZO nanoparticles, respectively. The filled blue and green squares and diamonds are for the 2D self-assembled Ag nanoparticles, and the red spheres are for 2D self-assembled YBCO nanoparticles. The inset shows $I_{c\text{-}w}(H)$ on a linear scale.

Conclusions

A range of nanoparticles has been investigated in order to increase flux pinning and critical current in YBCO films for high-current power applications. We found that the type of self-assembly of nanoparticles is important for enhanced critical current and that, for the chosen variety of nanoparticles and conditions of preparation, two-dimensional self-assembly is able to provide higher critical current in low magnetic field than a three-dimensional self-assembly.

Acknowledgements

Financial support of the European Commission through the Marie Curie Excellence Grant MEXT-CT-2006-041111 "NanoTechPinningHTS", ESF-NES Network and Romanian Ministry of Education and Research are gratefully acknowledged.

References

[1] Crisan A, Fujiwara S, Nie J C, Sundaresan A, Ihara H, Appl. Phys. Lett. 79, 4547 (2001).
[2] Haugan T, Barnes P N, Wheeler R, Meisenkothen F, and Sumption M, Nature 430, 867 (2004).
[3] MacManus-Driscoll JL, Foltyn S R, Jia Q X, Wang H, Serquis A, Civale L, Maiorov B, Hawley M E, Maley M P, and Peterson D E, Nat. Mater. 3, 439 (2004).
[4] Mikheenko P, Sarkar A, Dang V-S, Tanner J L, Abell J S, and Crisan A, Physica C 469, 798 (2009).
[5] Mikheenko P, Sarkar A, Dang V-S, Tanner J L, Awang Kechik M M, Abell J S, and Crisan A, IEEE Trans. Appl. Supercond. 19, 3491 (2009).
[6] Crisan A, Awang Kechik M M, Mikheenko P, Dang V S, Sarkar A, Abell J S, Paturi P and Huhtinen H, Supercond. Sci. Technol. 22, 045014 (2009).
[7] Awang Kechik M M, Mikheenko P, Sarkar A, Dang V-S, Hari Babu N, Cardwell D A, Abell J S, and Crisan A, Supercond. Sci. Technol. 22, 034020 (2009).
[8] Sarkar A, Mikheenko P, Dang V S, Abell J S, and Crisan A, Physica C, 469, 1550 (2009).
[9] Cherpak Yu V, Moskaliuk V O, Semenov A V, Svetchnikov V L, Tretiatchenko C G, Pan V M, Supercond. Sci. Technol. 20, 1159 (2007).
[10] Dubrovskii V G, Sibirev N V, Cirlin G E, Harmand J C, and Ustinov V M, Phys. Rev. E 73 021603 (2006).
[11] Yanagida T, Nagashima K, Tanaka H, and Kawai T, Appl. Phys. Lett. 91, 061502 (2007).
[12] Yamamoto H, Tsukamoto A, Saitoh K, Okada M and Kitaguchi H, Appl. Phys. Lett. 90, 142516 (2007).
[13] Maiorov B, Wang H, Foltyn S R, Li Y, DePaula R, Stan L, Arendt P N and Civale L, Supercond. Sci. Technol. 19, 891 (2006).
[14] Horide T, Matsumoto K, Ichinose A, Mukaida M, Yoshida Y and Horii S, Supercond. Sci. Technol. 20, 303 (2007).
[15] Maiorov B, Baily S A , Zhou H, Ugurlu O, Kennison J A, Dowden P C, Holesinger T G, Foltyn S R and Civale L, Nat. Mater. 8, 398 (2009).
[16] Goyal A, Kang S, Leonard K J, Martin P M, Gapud A A, Varela M, Paranthaman M, OIjaduola A, Specht E D, Thompson J R, Christen D K, Pennycook S J and List F A, Supercond. Sci. Technol. 18, 1533 (2005).
[17] Kang S, Goyal A, Li J, Gapud A A, Martin P M, Heatherly L, Thompson J R, Christen D K, List F A, Paranthaman M and Lee D F, Science 311, 1911 (2006).
[18] Gutiérrez J, Llordés A, Gázquez J, Gibert M, Romà N, Ricart S, Pomar A, Sandiumenge F, Mestres N, Puig T and Obradors X, Nat. Mater. 6, 367 (2007).
[19] Mele P, Matsumoto K, Horide T, Ichinose A, Mukaida M, Yoshida Y, Horii S and Kita R, Supercond. Sci. Technol. 21, 032002 (2008).

[20] Wee S H, Goyal A, Zuev Y L and Cantoni C, Supercond. Sci. Technol. 21, 092001 (2008).
[21] Zhou H, Maiorov B, Baily S A, Dowden P C, Kennison J A, Stan L, Holesinger T G, Jia QX, Foltyn S R and Civale L, Supercond. Sci. Technol. 22, 085013 (2009).
[22] Aytug T, Paranthaman M, Leonard K J, Kang S, Martin P M, Heatherly L, Goyal A, Ijaduola A O, Thompson J R and Christen D K, Phys. Rev. B 74, 184505 (2006).
[23] Miura M, Yoshida Y., Ichino Y, Takai Y, Matsumoto K, Ichinose A, Horii S and Mukaida M, Jpn. J. Appl. Phys., 45, L11 (2005).
[24] Yoshida Y, Ozaki T, Takai Y, Matsumoto K, Ichinose A, Horii S, Mukaida M, Journal of Physics: Conference Series 97, 012021(2008).
[25] Solovyov V F, Wiesmann H J, Wu L, Li Q, Cooley L D, Suenaga M, Maiorov B and Civale L, Supercond. Sci. Technol. 20, L20 (2009).